Electrochemical Microreactor for Chiral Syntheses Using the Cofactor NADH

Kane Cheikhou and Théodore Tzédakis
Laboratoire de Génie Chimique, UMR 5503, Université Paul Sabatier, 31062 Toulouse Cedex 04, France

DOI 10.1002/aic.11463
Published online March 28, 2008 in Wiley InterScience (www.interscience.wiley.com).

An electrochemical filter-press microreactor has been designed by electroerosion to perform chiral enzymatic syntheses. Semicylindrical channels are created in the electrodes, only separated by a Nafion membrane. Electrochemical and hydrodynamic characterization of the microreactor allows operating conditions to be optimized. Continuous enzymatic regeneration of NADH was achieved using flavin adenine dinucleotide ($FAD/FADH_2$) as redox mediator. The high specific surface area of the cathode (250 cm^{-1}) provides favorable conditions to increase the $FADH_2/FAD$ concentration ratio and shifts the nonspontaneous reaction $FADH_2/NAD^+$ toward regeneration of NADH. Synthesis of chiral L-lactate from pyruvate, in the presence of L-LDH, is the model reaction used to check the ability of the microreactor to regenerate NADH; the optimized device allows quantitative yields to be reached in NAD^+ conversion and in L-lactate production. The simulation (FemLab software) results are in good agreement with the experimental mass balances for flow in the range 0.1–0.2 cm^3/min. © 2008 American Institute of Chemical Engineers *AIChE J,* 54: 1365–1376, 2008
Keywords: electrochemical microreactor, chiral syntheses, NADH electrogeneration, modeling

Introduction

More than 300 dehydrogenases require the coenzyme nicotinamide adenine dinucleotide ($NAD(P)^+/NAD(P)H$) as cosubstrate.[1] Using NADH in preparative enzymatic synthesis[2] requires its continuous regeneration because of its high cost.

The efficiency of NADH regeneration can be quantified by TTN the total turnover number and TN the turnover number. In situ regeneration processes of NADH or NAD(P)H indicate values of TTN in the range 10^3–10^5 to be economically valuables.[3-5]

Several works deal with the regeneration of this coenzyme in various ways (chemically, photochemically, enzymatically, biologically, or electrochemically)[2,4–6]; it can, for example be carried out without enzymes, using chemical agents like sodium dithionite. Turnover number for NADH reaches 10 that is low; in addition, dithionite is a very reactive chemical against another enzymes.

Electrochemical regeneration of NADH can be performed directly at the electrode, in aqueous or no aqueous media, at relatively very cathodic potentials (−0.5 to −1.8 V/SCE) but the reaction leads to enzymatically inactive products.[7–11]

Electroreduction of NAD^+ bonded to the alginic acid is achieved by Aizawa et al.[12] Electrolysis during 20 h at −1.75 V/SCE allows to convert 50% of the initial NAD, and to limit loss of active NAD^+ to 5%.

Some enzymes allow direct electronic transfer without mediator. So, hydrogenases from *Rhodococcus opacus* and *Alcaligenes eutrophus* H16, were successfully used to regenerate NAD^+[13,14]and to transform the α-ketoglutarate to L-glutamate with TN lower than 450 h^{-1}. The overall reduction rate remains low and inappropriate for practical uses.

Electroregeneration of enzymatically active NADH or NAD(P)H can also be performed indirectly by using a redox mediator for electron transfer (Figure 1b). Various redox mediator (methyl viologen, flavins, quinonic compounds, and

Correspondence concerning this article should be addressed to T. Tzédakis at tzedakis@chimie.ups-tlse.fr.

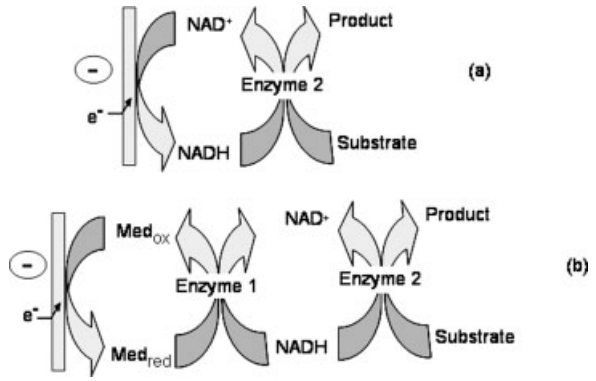

Figure 1. Schematic representation of chiral synthesis involving NADH cofactor, electrochemically regenerated (a) directly or (b) indirectly.

some ferrodoxins, rhodium complex),[9,15–19] assisted by various enzymes (ferrodoxin-NAD(P)$^+$-reductase,[20] lipoamide dehydrogenase,[9] formate dehydrogenase,[21] 2-oxocarboxylate and enoate reductases,[22] diaphorase, and alcohol dehydrogenase,[23]) have been used. In most cases TTN and TN remain lower than 1000 and 100, respectively; very often, the rate of the chemical reduction of NAD^+ by the mediator remains inappropriate to a real production. On the other hand, stability of some of these mediators is relatively low, and because of their toxicity, they are not useful for chiral syntheses.

Flavin adenine dinucleotide (FAD) is the mediator used in this study; it is a biologically relevant molecule as, physiologically, it promotes NADH oxidation in the respiration chain and other metabolic pathways[16]; it is also a mediator which minimizes side-reactions and has been reported to be biocompatible. Moreover, this mediator is also stable and reducible (1) for relatively high cathodic potentials, without negative effect on the enzymatic activity.[15] Nevertheless, the reduced form of flavin ($FADH_2$) can be very rapidly oxidized by dissolved O_2.

$$FAD + 2H^+ + 2e^- \rightarrow FADH_2 \qquad (1)$$

Thermodynamics favor NADH oxidation by FAD[15,16] according to the reaction (2) of which standard Gibbs energy ($\Delta G_2^\circ = -20.3$ kJ/mol) is negative. On the contrary, $\Delta G_{-2}^\circ = 20.3$ kJ/mol.

$$NADH + FAD + H^+ \underset{(-2)}{\overset{(2)}{\rightleftarrows}} NAD^+ + FADH_2 \qquad (2)$$

By using a thin-layer spectro-electrochemical cell (an analytical device), Bergel and Comtat [15] showed that it is possible to shift equilibrium (2) to the left, and hence to form NADH. Fine control of the working potential and a small volume ($\leq$100 μL) of electrolyzed solution increase the amount of flavin ($FADH_2$) electrogenerated in the thin layer cell. Consequently, thermodynamics (equation $\Delta G_2 = \Delta G_2^\circ + RT \ln \frac{[FADH_2]\cdot[NAD^+]}{[FAD]\cdot[NADH]\cdot[H^+]}$) show that a high ratio $[FADH_2]/[FAD]$ causes the Gibbs energy of the reverse reaction (ΔG_{-2}) to become negative and the equilibrium shifts toward NADH (Eq. 2). Turnover numbers higher than 1400 were obtained for the reduction of pyruvate to L-lactate, with this system, so this is the main reason of the choice of FAD in this work. If a few examples of electrochemical microreactors for synthetic applications, have been reported,[24–27] electrochemical microreactors have never been used, to regenerate NADH coenzyme using flavin adenine dinucleotide.[17,18]

A microreactor adapted for syntheses could be defined as a series of interconnecting channels (10–300 μ in diameter) created in a flat surface in which small quantities of reagents are manipulated. The main feature of these devices,[25,26] i.e., their surface area to volume ratio (lies between 20 and 1000 cm^{-1}), very high in comparison with these of traditional reactors ($\sim$1 cm^{-1}), cause the mass transfer and heat transfer to significantly improve.

There are many methods for micro- and nanofabrication; even if lithography is the most wide-spread,[28] cylindrical shapes are quite difficult to generate with this technique. In this work, electroerosion was used to manufacture the microreactor.

The aim of this study was to demonstrate that our electrochemical microreactor is able to regenerate continuously NADH from NAD^+, using Flavin as redox mediator and a formate dehydrogenase enzyme. Synthesis of L-lactate from pyruvate (Figure 1b) is the enzymatic model reaction (3) chosen to confirm the feasibility of the NADH regeneration.

$$NADH + Pyruvate \overset{L-LDH}{\rightleftarrows} NAD^+ + L - Lactate \qquad (3)$$

Theoretical simulation of the electrochemical microreactor was performed by using commercial software, to compare experimental results to theoretical ones and to validate the elaborated tool, requested to the theoretical optimization of this complex system.

Experimental

Chemicals

The chemicals used were purchased from Acros, Sigma-Aldrich, Merck, or Prolabo. The enzyme L-lactate dehydrogenase (L-LDH) is from rabbit muscle, and the formate dehydrogenase (FDH) from yeast *Candida bodinii*.

Apparatus

In a previous work,[17] we presented the design and production of the filter-press microreactor (Figure 2). Two rectangular plates (5 cm $\times$ 5 cm $\times$ 0.2 cm), made of gold and platinum, are used as cathode and anode, respectively. One hundred thirty semicylindrical channels (diameter 160 μm) were made by electroerosion on one face of each plate, so their specific area reaches 250 cm^{-1}. Two large channels (3 mm $\times$ 0.7 mm $\times$ 40 mm), located at the bottom and at the top of the metal plate, provide uniform distribution of electrolyte to all microchannels as well as uniform output of the electrolyzed solutions. The anode is separated from the cathode by a Nafion proton exchange membrane N1135. The hydraulic connection tubes, made in the same material as the electrodes, were welded to the backs of the electrode plates. A platinum wire inserted into a Teflon pipe, which opens into the large electrolyte inlet channel, is used as the comparison electrode. The assembled reactor was then housed in a watertight Teflon casing. Figure 2 provides a representation of the whole apparatus used for the mass balance experiments.

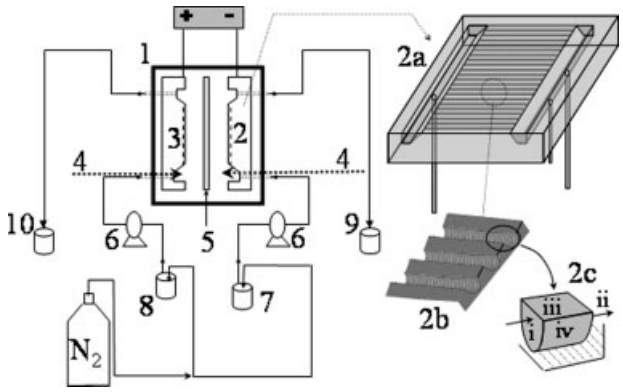

Figure 2. Scheme of the apparatus used for mass balance experiments.

1: Filter-press microreactor; 2, 2a, 2b, and 2c: cathode (Au) and enlarged microstructured surfaces; 3: anode (Pt); 4: Pt wire used as comparison electrode; 5: Nafion membrane; 6: peristaltic pump (Watson-Marlow 2058); 7 and 8: catholyte and anolyte feeds; 9 and 10: catholyte and anolyte recovery after electrolysis. 2c: Schematic representation of a slice of the microchannel with semi cylindrical shape; (i) inlet face; (ii) outlet face; (iii) membrane face; (iv) electrode face.

Theoretical Simulation of the Microreactor

Simulations of various experiments were performed with FemLab software to propose a theoretical model for the microreactor by taking in account:

-the electrochemical reaction (1),

-both reactions (1) and (2), i.e., NADH regeneration, and

-the overall reaction scheme described in Figure 1b, reactions (1)–(3).

Expected results are the concentration profiles for various species as well as the conversion of reagents like NAD^+ and pyruvate. A further objective was to demonstrate the feasibility within the microreactor of a thermodynamically nonfavored reaction, leading to the formation of a chiral product.

Equations are discretized by the finite element method. As indicated in Figure 2, electrodes are equipped with two holes (for inlet and outlet solutions) located in the middle of the main (top and bottom) channels. The velocity profile is nonuniform in the microchannels because of the pressure drop in the main channels, but to simplify calculations, every microchannel was assumed to have the same velocity profile and same composition, so simulation was done in one microchannel.

*Navier-Stokes equations (4) are coupled with steady-state convection-diffusion equation (5) to simulate the microreactor.

$$\begin{cases} \rho\left[\dfrac{\partial \vec{V}}{\partial t} + (\vec{V}\cdot\nabla)\vec{V}\right] = -\vec{\text{grad}}\, p + \mu\nabla^2\vec{V} + \rho\vec{g} \\ \nabla\vec{V} = 0 \end{cases} \tag{4}$$

$$^*\text{Convection} - \text{diffusion equation for species } j\text{:}\quad \nabla(-D\cdot\nabla c_j + c_j\cdot V) = R_j \tag{5}$$

where R_j is the overall rate of all homogeneous reactions occurring in the bulk solution. Expressions of R_j for species FAD, $FADH_2$, NAD^+, NADH, pyruvate, and L-lactate are R_{-2}, $-R_{-2}$, R_3–R_{-2}, R_{-2}–R_3, $-R_3$, and R_3, respectively.

Migration terms are neglected because of the presence of a supporting electrolyte, i.e., phosphate buffer.

Boundary conditions

Because of the semicylindrical shape of the microchannels (Figure 2c) some additional simplifications were made, and by this way various boundary conditions can be used.

There are some common boundary conditions (hydrodynamics) as follows:

*An uniform flow is established at the face i and at any point of this face, flow will be characterized by the average velocity, determined by the ratio volumetric flow to channel cross sectional area. Calculations of the distance (L) from the entrance necessary to obtain a uniform stream were performed using relationship: $L = 0.06 \times d_h \times Re$, where d_h is the hydraulic diameter and Re the Reynolds number (calculated with the average velocity).[29] Results show that the L value represents 0.02% of the total length of the microchannel (4 cm).

*Flux for electroactive species on face iii, i.e., the electrolyte separator, is zero except for hydrogen ion from the anode to the cathode. In this study, pH remained constant in both compartments because of the concentrated phosphate buffered solution.

*On face ii, the electrochemical reaction is assumed to be finished because the electrode area is interrupted, or because conversion of electroactive species is complete. In these conditions there is no current, so no consumption and consequently neither diffusion nor migration takes place. In the case of the microreactor studied here, this is an oversimplification, because at the end of each individual microchannel there is a relatively large channel; it works both as a collector of various streams, and also as an electroactive surface on which electrochemical reactions can be pursued. Nevertheless, electrochemical conversion in this relatively large channel is very low because its volume is large in comparison with its small surface area. This assumption is therefore justified.

*On face iii and iv, shear stress is maximal, or velocity is null.

Two specific boundary conditions can be used at the electrode surface, face iv, Figure 2c:

*The sum of the flux of oxidized and reduced forms is zero ($N_{ox} = N_{red}$) at the electrode.

*Calculations can be performed making two additional assumptions:

(a) There is no limitation by electron transfer, and only mass transfer governs the flux at the electrode. In this case, simulation implies knowing the average value of the mass transfer coefficient K_{av}, then the mass flux density at the electrode is given by $N_j = K_{av}\cdot c_j^\circ$, where c_j° is the inlet concentration of electroactive species.

(b) Limitation to the overall process can be provided by both electron and mass transfer; in this case, to access the flux density ($N_j = \frac{i}{n\cdot F}$), the Butler-Volmer equation was used for the current density expression as follows:

$$i = i^\circ\cdot\left[\frac{c_{ox}^{elec}}{c_{ox}^{bulk}}\cdot\exp(-\alpha\cdot\frac{n\cdot F}{RT}\cdot\eta) - \frac{c_{red}^{elec}}{c_{red}^{bulk}}\cdot\exp((1-\alpha)\cdot\frac{n\cdot F}{RT}\cdot\eta)\right] \tag{6}$$

η is the overpotential, i.e., the difference between applied potential and the zero current potential.

F is the Faraday constant, R is the gas law constant, i_0 is the exchange current–density, c_{ox}^{elec} and c_{red}^{bluk} are the concentration at the electrode and in the bulk solution, respectively, for the oxidized or the reduced form. $i_\circ$, the exchange current–density and α, the cathodic transfer coefficient are determined in the kinetic section.

Theoretical simulations for the overall process described in Figure 1b were carried out by taking into account convection-diffusion equation (5) for all species j.

Let us note that, in this theoretical study, inhibition of FDH by various reagents, particularly by NAD^+ can be ignored[30] because of the low concentrations used ($[NAD^+] < 10$ mM).

The diffusivity value used for NADH is 2.4×10^{-10} m^2/s, and NAD^+ is assumed to have the same diffusivity.[31] For L-lactate diffusivity is 1.06×10^{-9} m^2/s, and pyruvate is assumed to have the same diffusivity.[32]

Results

Enzyme assay

The specific activity of enzymes FDH from the yeast *Candida bodinii and* L-LDH from rabbit muscle were determined by UV measurements, according to the analytical method described in the Annex 1a; their values were found to be 0.92 U_{FDH}/mg and 866 U_{LDH}/mg, respectively, for FDH and LDH.

Spectrophotometric and chromatographic measurements

Flavin (FAD) and NADH samples were analyzed by UV spectrophotometer according to the analytical method described in the Annex 1b. The determination of the NADH concentration in the electrolyzed solution needs two coupled measurements of absorbance at 450 and 340 nm; the combination of these values allows the NADH concentration to be determined with an incertitude lower than 4%.

L-Lactate concentration was determined by HPLC according to the analytical method described in the Annex 1c. The incertitude to this measurement led to an error on the L-lactate concentration lower than 5%.

Characterization of the microreactor

The goal is to define the optimum operating conditions, to study and solve practical questions related to the nature of the reagents used, and to determine various physical parameters necessary for theoretical simulations.

On the hydrodynamic point of view, in general, for flow in a channel of diameter greater than 41 μm, there are no specific contributions of pressure drop to take into account.[29,33] This is in agreement with experiment; for all preparative electrolyses without evolution of hydrogen or oxygen, the pressure drop remains lower than 10^5 Pa.

To characterize the microreactor, electrochemical experiments were achieved using the reversible hexacyanoferrate III/hexacyanoferrate II redox system (7), and kinetic parameters, optimal flow conditions, as well as the mass transfer of ferricyanide were determined.

$$Fe(CN)_6^{3-} + e^- \rightleftarrows Fe(CN)_6^{4-} \quad (7)$$

The curves obtained by cyclic voltammetry in the transient state, without flow (not showed), indicate a classical shape for a quasi-reversible electrochemical system. The relatively high difference between the peaks potentials $\{\Delta E_{peak} = 0.031 - (-0.138) = 169$ mV$\}$ is caused by the "comparison electrode" used. Indeed during the scanning, electrolysis modifies the ferricyanide/ferrocyanide ratio in the inlet area of the electrode, and consequently the potential of the comparison electrode. The magnitude of the oxidation current is about 90% of the corresponding value for the cathodic curve, because of the slight difference of the diffusivities between reduced and oxidized form.

To determine the average value of the mass transfer coefficient K_{av}, current–potential curves were plotted (Figure 3a) for steady-state conditions with various flow rates. The curves indicate that reduction of ferricyanide takes place for potentials lower than -0.1 V; the shape of the curves strongly depends on the flow rate; indeed, when it is lower than 3 cm^3/min (curves 1–3), the reduction signal has the shape of a peak; ferricyanide reduction current decreases with the potential due to the concentration depletion in the microchannel; the high specific area of this microreactor allows operation under high conversion rates.

When flow rate becomes higher than 3 cm^3/min, classical shaped curves are obtained indicating a limiting current, constant, over the potential range -0.15 to -0.3 V; in fact, a small residence time does not allow high conversion of ferricyanide, and a constant concentration in the "bulk" of the microchannel leads to a constant current.

The cathodic transfer coefficient α, as well as the exchange current–density of ferricyanide reduction on the gold cathode (i°) were determined experimentally by logarithmic analysis

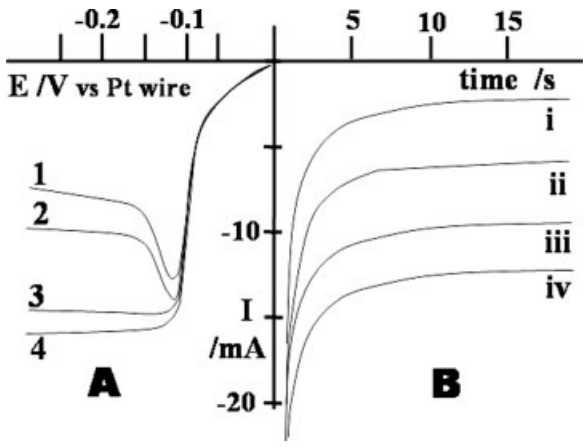

Figure 3. Electrochemical measurement carried out using a filter-press microreactor, with various flow rates of a ferricyanide 5 mol/m³ solution.

Cathode = Au; anode = Pt; 0.01 V/s; $S_{Au} = S_{Pt} = 1.3 \times 10^{-3}$ m^2; 298 K; $N_2 = 10^5$ Pa. (A) Current potential curves obtained for various flow rate: 0.95, 1.6, 2.8, and 4.3 cm^3/min for curves 1, 2, 3, and 4, respectively. (B) Chronoamperograms obtained at $E = -0.2$ V/Pt wire for various flow rates: 0.26, 1.1, 2.2, and 3.5 cm^3/min for curves i, ii, iii, and iv, respectively.

of current potential curves 3 and 4 (Figure 3a). Their values are $i^\circ = 0.3$ A/m^2 and $\alpha = 0.5$.

Unfortunately, the available flow range allowing a "constant" limiting current is small (3–5 cm^3/min) because of leakages of solution for "high" flow. Consequently, to determine the average value of the mass transfer coefficient K_{av} chronoamperometric measurements, at a constant potential of -0.2 V applied to the gold cathode, were performed for various flow rates over the range 0.2–3.5 cm^3/min (Figure 3b). The algebraic current decreased with time and reached a practically constant value for all flows examined. Let us note that for higher flows this steady-state current corresponds to the limiting current.

To determine the average mass transfer coefficient the following assumptions will be made:

– the measured steady-state current density obeys to the classical relation: $i = n{\cdot}F{\cdot}K_{av}{\cdot}c$.

– the microreactor can be assimilated to a plug flow reactor, so under potentiostatique conditions, the concentration varies exponentially with the channel length x: $c = c^\circ{\cdot}\exp\{-\pi{\cdot}r{\cdot}K_{av}{\cdot}x/Q\}$, where r is the radius of the hemicylindrical microchannel.

– the overall measured current I is given by the integral of the current density i: $I = \int_{x=0}^{x=1} \pi r\ nFK_{av} \cdot c^o \exp(-\frac{\pi r K_{av}{\cdot}x}{Q})dx$.

In these conditions, the following relationship describes the flow rate dependence of the average value of the mass transfer coefficient:

$$K_{av} = -\frac{Q}{S}\ln\left(1 - \frac{I}{nFc^oQ}\right) \tag{8}$$

The analysis of the experimental chronoamperometric measurements (Figure 3b) provides the requested $K_{av} = f(\text{flow})$ empiric correlation (9).

$$K_{av} = 0.152{\times}Q^{0.57} \tag{9}$$

K_{av} and Q are expressed in (m/s) and (m^3/s), respectively.

Electrochemical behavior of various chemicals used for L-lactate synthesis

Figure 4 presents the cathodic part of the voltammograms, obtained in the transient state, for the various chemicals used in L-lactate synthesis. The curves show no reaction before about -0.7 V/Pt wire for any species except flavin.

The Curves 3 and 4 in the range examined are similar to those of the residual current (1) except for a slight shift to cathodic values, probably caused by partial passivation of the cathode owing to the presence of L-lactate and pyruvate.

Curve (2) shows that FAD can be reduced at the cathode for potentials lower than -0.4 V, and the cyclic voltammetry signal has a classical shape. Nevertheless, various results show that it is not very easy to obtain reproducible voltammograms; indeed phenomena such as adsorption, acid/base equilibrium shifts, and electrochemical reduction of flavin can take place affecting the magnitude of the signal and the number of peaks/shoulders.[34]

Logarithmic analysis of the experimental current–potential curve obtained in the steady state with 5 mol/m^3 flavin in phosphate buffer pH 7.0, provided kinetic parameters, useful for theoretical simulations, like the exchange current density

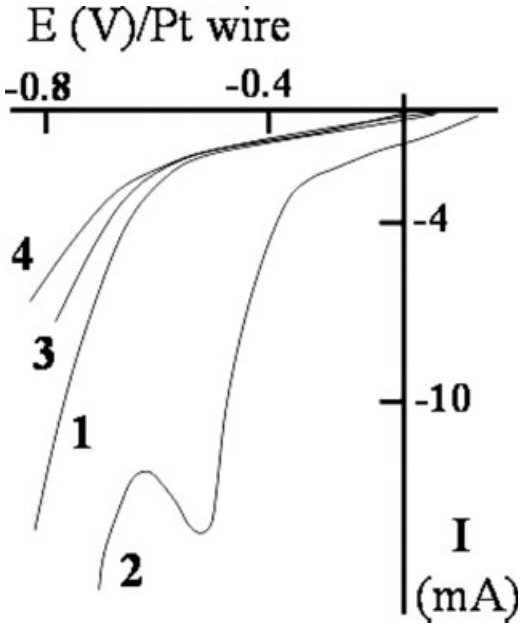

Figure 4. Current–potential curves obtained in the microreactor for various chemicals used in L-lactate synthesis.

Phosphate buffer pH = 7.0; cathode = Au; anode = Pt; $S_{Au} = S_{Pt} = 1.3 \times 10^{-3}$ m^2; 0.1 V/s; 293 K; $N_2 = 10^5$ Pa; No flow in the microreactor. (1) Residual current; (2) [FAD] = 3.85 mol/m^3; (3) [L-Lactate] = 4 mol/m^3; (4) [Pyruvate] = 7 mol/m^3.

i_0 as well as the electron transfer coefficient α, of flavin on the gold cathode: $i_0 = 2.25 \times 10^{-2}$ A/m^2, $\alpha = 0.14$ assuming two electrons for flavin reduction.

Diffusivity, D, of FAD was determined by various chronopotentiometric experiments[35]: in a phosphate-buffered solution $D_{[FAD]=5.3\ mol/m^3} = 0.82 \times 10^{-10}$ m^2/s; note that this value is relatively low because of the "large" size of the FAD molecule, and can vary with its concentration.

Determination of the kinetic parameters for the chemical reactions

The enzymatic reaction (-2) between reduced flavin $FADH_2$ and nicotinamide adenine dinucleotide NAD^+ is an ordered reaction,[36,37] and its kinetics obeys to the relationship (10) as follows:

$$R_{-2} = \frac{R_{max-2}}{1 + K_{-2} + \frac{K_{mFADH_2}}{[FADH_2]} + \frac{K_{mNAD^+}}{[NAD^+]}} \tag{10}$$

Some kinetic parameters of this reaction ($NAD^+/FADH_2$) have been estimated by Bergel and Comtat[15] particularly the Michaelis-Menten constant $K_{mFADH_2} = 9$ mM. In addition, for experiments carried out with concentrations of species lower than 10 mM, it is assumed that the mixed inhibition constant is null. In this work, all concentrations were lower than 10 mM, so $K_{-2} = 0$.

R_{max-2} is the maximum velocity $= k_{cat-2}{*}[FDH]^\circ = 0.1$ mol/(m^3 s) for $[FDH]^\circ = 5$ U/cm^3.

A ratio of 1.3×10^{-2} was deduced between the activity of the enzyme FDH with respect to this process and its normal

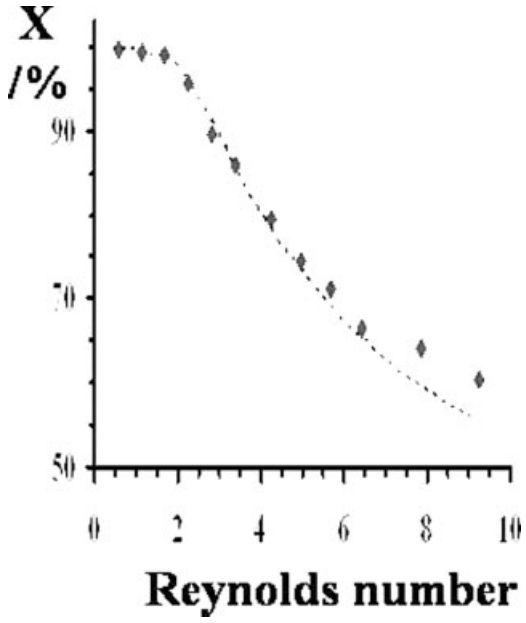

Figure 5. Ferricyanide conversion vs. Reynolds number.

Mass balance experiments performed in the microreactor under potentiostatic conditions. $E_{applied} = -0.2$ V/Pt wire, [KCl] = 200 mol/m^3; 293 K; $N_2 = 10^5$ Pa; [ferricyanide]$^\circ$ = 5 mol/m^3; $Q_{catholyte} = Q_{anolyte}$; no recycling. ♦♦♦♦, Experimental conversion; ...., Simulated conversion when Butler-Volmer equation is used to calculate mass flux density.

activity with respect to formate (Annex 1a). This ratio was determined in a thin layer electrochemical cell, which is quite different from the microreactor used here. A numerical correction of the enzyme concentration was made. In particular, the FDH concentration was chosen related to formate reduction (Annex 1a).

The enzymatic reaction between reduced nicotinamide adenine dinucleotide NADH and pyruvate (3) obeys an ordered Theorell-Chance mechanism; its kinetics can be modeled[30] as follows:

$$R_3 = \frac{R_{max3}}{1 + K_3 + \frac{K_{m\,NADH}}{[NADH]} + \frac{K_{m\,Pyruvate}}{[Pyruvate]}} \quad (11)$$

where R_{max3}: maximum velocity = k_{cat3}*[L-LDH]$^\circ$ = 0.02 mol/(m^3 s) for [L-LDH] = 0.05 U/cm^3,

k_{cat3} is the catalytic constant[30] = 1.7 s^{-1},

$K_3 = 1.38 \times 10^{-3}$ mixed inhibition constant between NADH and pyruvate,

Michaelis-Menten constants: $K_{m\ pyruvate}$: 1.6×10^{-6} mol/L; $K_{m\,NADH} = 10.7 \times 10^{-6}$ mol/L.

Mass balance experiments

(a) Study of the Microreactor Performance Using Ferricyanide Solution. Electrolyses, carried out under potentiostatic conditions, and the residual concentration of ferricyanide after electrolysis in the microreactor, was determined by UV spectrophotometry at 420 nm. Applied potential at the cathode allows operating under the limiting current, so theoretically the rate of secondary cathodic reactions is practically cancelled. Figure 5 indicates the conversion of ferricyanide vs. the *Re* number.

Quantitative conversion of substrate was obtained for *Re* number lower than = 1.5 (flow < 1 cm^3/min). Increasing flow leads to decreased conversion of ferricyanide because the residence time and consequently the amount of charge passed, decrease: 50% of the ferricyanide was converted for a relatively high flow rate of 5 cm^3/min corresponding to a *Re* number of 11.3. This is the maximum flow rate tolerated by the microreactor before leakage. For all electrolyses, the Faradic yield remains in the range of 94 and 96%, a result in agreement with the absence of hydrogen bubbles in the catholyte.

Theoretical simulations were carried out for the ferricyanide/ferrocyanide system, to validate the experimental results obtained for the characterization of the microreactor. In this case, there was no chemical reaction in the bulk ($R_j = 0$). Simulation provides first the velocity profile in the microchannel; a classical parabolic shape was obtained showing that the laminar flow is well developed in the microchannel and the inlet effect can be neglected.

The theoretical conversion of ferricyanide, obtained using the Butler-Volmer equation (6) as a boundary condition, is plotted vs. *Re* number in Figure 5, alongside experimental values (black squares). Agreement between experimental and theoretical results is satisfactory for *Re* number lower than 6 (i.e., flow rates < 3 cm^3/min); a small deviation is observed for higher flows. The Butler-Volmer equation includes parameters difficult to evaluate precisely for high values of overpotential (such as the interfacial concentration or an exponential term which tends to infinite); so using this relation as a boundary condition could lead to uncertain results, explaining discrepancies between theory and experience.

(b) NADH electroregeneration

Experimental Results

Influence of the volumetric flow. To study the regeneration of NADH within the microreactor, mass balance experiments were carried out under potentiostatic conditions, for flow rate lower than 0.5 cm^3/min.

Electrolyses reduce FAD to $FADH_2$ (1), then chemical reaction (−2) can take place and produce NADH, the desired compound. Results indicated in Figure 6 (black squares, 1), which presents the *Re* number dependence in the experimental conversion of NADH. Relative high conversion yields of NAD^+ to NADH (>50%) can be obtained for flow rate of 60 μL/min corresponding to a residence time of 45 s, and a *Re* number close to 0.1.

Increasing the flow rate causes a decrease of NAD^+ conversion. Indeed, the low residence time[35] of the mixture ($FADH_2/NAD^+$) does not allow to fully develop the chemical reaction (−2). To demonstrate it three successive electrolyses are carried out with the same solution.

Analysis of electrolyzed solution (Table 1), performed about 10 min after the end of electrolyses, indicate that:

*Absorbance at 450 nm remain constant, meaning that on the one hand concentration of oxidized form of Flavin remain constant (5.14 mmol/L) and on the other hand reduced form of Flavin ($FADH_2$) is absent to the electrolyzed solution because of its instability. Consequence of this is that

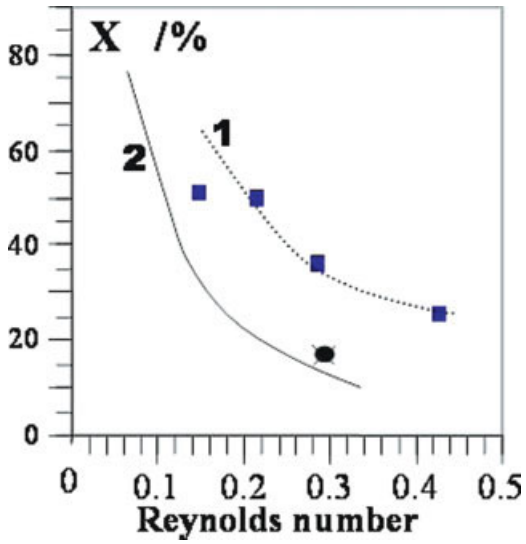

Figure 6. Conversion X of NAD^+ to NADH (1) and pyruvate to L-lactate (2) against Reynolds number.

Mass balance performed in the microreactor. Phosphate buffer pH = 7.0; applied overpotential $\eta = -0.5$ V; 298 K; $N_2 = 10^5$ Pa; $Q_{anolyte} = Q_{catholyte}$. Curve 1: $[FAD]^\circ = 5$ mol/m^3; $[NAD^+]^\circ = 3$ mol/m^3; $[FDH]^\circ = 5$ U/cm^3; dashed line: simulation results; ■■■■ experimental results. Curve 2: $[FAD]^\circ = [NAD^+]^\circ = 4$ mol/m^3; [pyruvate]$^\circ = 3$ mol/m^3; $R_{max-2} = 0.1$ mol/(m^3 s^1), $R_{max3} = 0.02$ mol/(m^3 s^1). Continuous line: simulation results; ●: experimental result (Run 1, Table 2). [Color figure can be viewed in the online issue, which is available at www.interscience.wiley.com.]

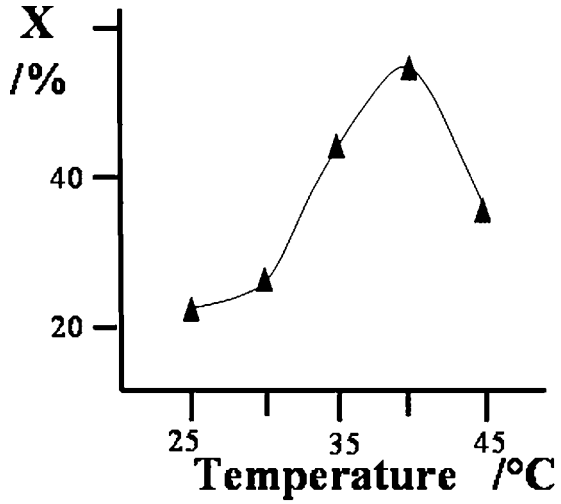

Figure 7. Conversion of NAD^+ to NADH vs. temperature.

$[NAD^+]^\circ = [FAD]^\circ = 4$ mol/m^3; $[FDH]^\circ = 0.0945$ U/cm^3; electrolysis at -0.55 V/Pt wire; $Q_{anolyte} = Q_{catholyte} = 0.126$ cm^3/min.

the effect of the mass transfer is negligible in comparison with the effect of the residence time in the progression of reaction (−2) in the direction of NAD^+ conversion.

*Recycling three times (discontinuously) the electrolyzed solution enables 100% conversion of NAD^+ to NADH.

*Current efficiency, estimated vs. indirect electroregenerated NADH remains close to 20%. Taking account that electrolyses are performed under potentiostatic conditions, faradic yield for $FADH_2$ has to be close to 90%, because 10% of the current is attributed to the water reduction (Figure 4). Nevertheless, loss in the reduced form of flavin ($FADH_2$) drastically decreases the current efficiency of the overall process.

Let us note that for electrolyses under galvanostatic conditions, the correlation "current against volumetric flow" must be known, to estimate the optimum value of the current to apply[35] and consequently to operate under with the maximum faradic yield (close to 100%).

Influence of the temperature. The influence of the temperature on the experimental conversion of electroregenerated NADH was examined and the results of the preparative electrolyses, reported in Figure 7, show that NAD^+ conversion first increases from 20 to 40°C, and decreases for higher temperature.

Various parameters can cause this evolution; theoretically, diffusivity of FAD (and consequently the magnitude of its reduction current) increases when the temperature increases and led to a higher concentration of $FADH_2$; nevertheless, as previous results shown, the electrolyzed solution does not contain $FADH_2$ and conversion of NAD^+ was not quantitative. In addition, the activation energy of the mass transfer phenomenon is in general lower than the activation energy of a chemical reaction.[38] In this case, the activation energy of the overall phenomenon (Reactions 1 and 2) can be estimated from data of Figure 7, assuming that the overall rate can be approximated by the ratio $d[NADH]_{outlet}/dt = X^*[NAD^+]^\circ/\tau = \text{constant}^*\exp(-E_a/RT)$.

Results led to the following relationship: $\ln(X^*[NAD^+]^\circ/\tau) = -6443/T + 8.954$; $R^2 = 0.98$, so an activation energy (E_a = 53.5 kJ/mol) relatively high, indicating that increasing temperature mainly acts on the chemical reaction (−2) and shift it toward NADH regeneration. Moreover, influence of the increase of the current by temperature effect, on the NAD^+ conversion, will be assumed as negligible.

In fact, temperature seems to mainly influence the FDH enzymatic activity; indeed, according to Slusarczyk,[39] the

Table 1. Mass Balances for Electro-Enzymatic Regeneration of NADH Performed Under Potentiostatic Conditions

Recycling Stages	A_{340} (×100 diluted)	A_{450} (×100 diluted)	X_{NAD+} (experimental analysis)	Faradic yield (%): $\frac{2F\cdot flow\cdot C^\circ_{NAD^+}\cdot\tau\cdot X_{NAD^+}}{\int_0^t I\cdot dt}$
0	0.1883	0.404	0	0
1	0.2668		30	16
2	0.3611		66	21
3	0.4501		Quantitative	23

$[FDH]^\circ = 0.5$ U/cm^3; $[FAD]^\circ = 5.14$ mmol/L; $[NAD^+]^\circ = 5.70$ mmol/L; phosphate buffer: 50 mol/m^3; pH = 7; initial volume of the electrolyzed solution: ~1 cm^3; flow = 63 μL/min; $\tau = 50$ s; applied overpotential $\eta = -0.5$ V; N_2 10^5 Pa; 293 K.

optimal activity of formate dehydrogenase is reached at temperature close to 45°C, and this is in agreement with the results of this work. Activity of FDH as well as NAD^+ conversion increases until about 40°C and decreases to 35% for temperature that reach 50°C.

Simulation results. Theoretical simulations were carried out for the reaction scheme including both electrochemical (1) and enzymatic steps (−2), i.e., the indirect electroregeneration of NADH by mediation of a flavinic cofactor.

As explained previously, the homogeneous reaction (2) between FAD and NADH is spontaneous. Using microstructures, created directly in the electrode, decreases the size of the electrolyte stream practically to the thickness of a "classical" value of diffusion layer, i.e., $\sim 10^{-3}$ cm. A uniform concentration profile is assumed to exist at any point in the stream, and the concentration ratio [reduced Flavin]/[oxidized Flavin] can be increased; the consequence of this phenomenon is to shift the $NAD^+/FADH_2$ equilibrium toward NADH regeneration, a situation similar to that of the thin layer cell.[15] The main objective of this part of the study was first to demonstrate that using small microstructures allows operation with negative free enthalpy; another objective was to determine the concentration profiles and the conversion for species within the microreactor to optimize the overall electrogeneration process of the pyridinic cofactor.

The dimensionless concentration profiles for all species obtained in the microchannel are presented in Figure 8a. The results show that conversion rate of FAD to $FADH_2$ exceeds 90%, after one residence time in the microreactor.

The flavin concentration ratio ($[FADH_2]/[FAD]$) is plotted in the same graph vs. the channel length, graph (b); the curve has a sigmoidal shape, which means that the reaction (1) progressed faster in the first part of the channel.

Moreover, Curves 3 and 4 in Figure 8a clearly indicate that NAD^+ is reduced to NADH; theoretical conversion for one residence time (4 cm of the length) is over 50%.

Figure 9, graph (a) plots the Gibbs energy ΔG_{-2} against microchannel length, calculated using the following relationship:

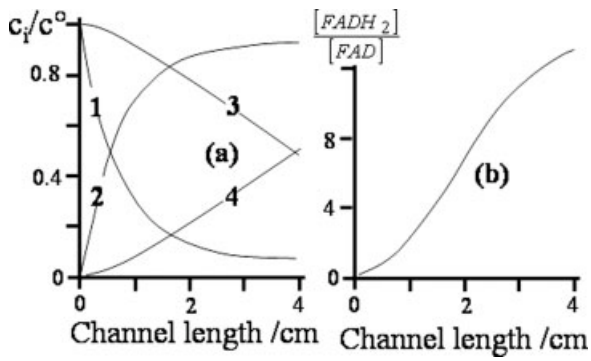

Figure 8. Simulated results of electrolyses performed using a filter press microreactor.

$[FAD]^\circ$ = 5 mol/m^3; $[NAD^+]^\circ$ = 3 mol/m^3; $[FDH]^\circ$ = 5 U/cm^3; R_{max-2} = 0.1 mol/(m^3 s); $Q_{anolyte} = Q_{catholyte}$ = 0.0945 cm^3/min. (a) Dimensionless concentration as a function of the microchannel length for all species, i.e., 1: FAD, 2: $FADH_2$; 3: NAD^+, 4: NADH. (b) Evolution of the simulated ratio $[FADH_2]/[FAD]$ within the microreactor.

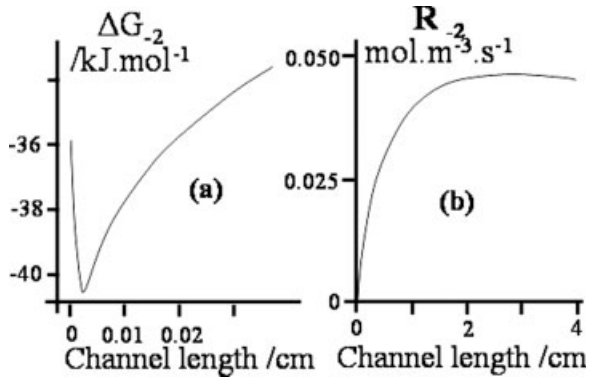

Figure 9. Theoretical evolution of free enthalpy (a) and chemical reaction rate R_{-2} (b) against the microchannel length, during electrolyses within a microreactor.

$[FAD]^\circ$ =5 mol/m^3; $[NAD^+]^\circ$ = 3 mol/m^3; R_{max-2} = 0.1 mol/(m^3 s); $Q_{anolyte} = Q_{catholyte}$ = 0.0945 cm^3/min.

$$\Delta G_{-2} = 20,300 + RT \ln \frac{[FAD] \cdot [NADH] \cdot [H^+]}{[FADH_2] \cdot [NAD^+]} \qquad (12)$$

where $^*\Delta G^\circ_{-2} = 20,300$ J/mol (or $\Delta G^\circ_2 = -20,300$ J/mol) is the standard free enthalpy of the homogeneous reactions (2) or (−2), arises from calculation from standard states thermodynamic values.

*The concentrations are expressed in mol/L.

Gibbs energy is a function of the flavin concentration ratio $\frac{[FAD]}{[FADH_2]}$, and the results indicate that at pH = 7 and for lengths of over a few micrometers, the Gibbs energy becomes negative at all points within the microchannel. Let us note that, in this study relatively low concentrations (<5 mM) solutions are involved, so we can assume that the activities are similar to the concentrations.

The curve can be separated into two parts: for lengths lower than 50 μm Gibbs energy strongly decreases algebraically down to −40 kJ/mol, because of the electrolytic production of the reduced form of flavin, which causes an increase in the concentration ratios $\frac{[FADH_2]}{[FAD]}$ and $\frac{[NADH]}{[NAD^+]}$. Comparison of this results with the graph (b) of Figure 8 indicate that the backward reaction (−2) is thermodynamically favored for even low concentration ratios $\frac{[FADH_2]}{[FAD]}$. Simultaneously, graph (b) of Figure 9 shows that the rate of the backward reaction (−2) increases because of $FADH_2$ formation.

In the second part of curves (a) and (b) in Figure 9, Gibbs energy as well as the chemical rate R_{-2} seems to be stabilized, [at −35 kJ/mol and 0.045 mol/(m^3 s), respectively] because a steady state is reached for the overall process: electrochemical production/chemical consumption of $FADH_2$. Note that to attain the highest production it is important to optimize the flow and the concentrations that allow operation at maximum rate immediately at the inlet of the microchannel.

Figure 6 (dashed line, Curve 1) plots the theoretical conversion of NAD^+ to NADH vs. the *Re* number. Comparison with experimental results (black square) is in good agreement for $Re > 0.2$, but discrepancies appear for lower flows;

Table 2. Mass Balances for Electro-Enzymatic Synthesis of L-Lactate from the Pyruvate Performed Under Various Operating Conditions

Run No.	1	2*	3**	4**
[Sodium pyruvate]$_0$ (mol/m^3)	2.89 ± 0.05		1.38 ± 0.05	
[FAD]$_0$ (mol/m^3)	3.94 ± 0.05	4.11 ± 0.05	4.81 ± 0.05	
[β-NAD$^+$]$_0$ (mol/m^3)	3.91 ± 0.05	3.84 ± 0.05	4.04 ± 0.05	
[LDH]$_0$ (U/cm^3)	2	5		0.5
$Q_{anolyte} = Q_{catholyte}$ (m^3/s^1)	21.7×10^{-10}	5.3×10^{-10}	10.7×10^{-10}	
Residence time (s)	23	73	137	
Conversion of pyruvate to L-lactate (%)	23	36	~100	~100
Turnover number (H^{-1})	27	13	9	9
Production of L-lactate [mol/(m^2 day)]	0.12	0.05	0.13	0.13

$E_{applied}$: −0.6 V/Pt wire; phosphate buffer: 50 mol/m^3; pH = 7; N_2 10^5 Pa; 293 K; [FDH]$_0$ = 0.5 U/cm^3.
*Catholyte continuously recycled into the microreactor (recycling rate = 0.25).
**Catholyte recycled three times, as a whole batch each time, into the microreactor.

experimental conversion seems to be stabilized while theoretical conversion increases continuously. Reducing the flow, increases the residence time and causes a continuous increase of the theoretical conversion of NAD^+. In contrast, the behavior of experimental conversion can be explained by the internal structure of the microreactor: the nonoptimized shape and skew of the main channels (distributing and collecting) cause the presence of dead areas in the microreactor. The consequence is a drop of available electrochemical area and also a decrease of the $FADH_2$ concentration. Another explanation of discrepancies is that the simulation does not take account the instability of $FADH_2$.

To sum up, the theoretical model of NADH regeneration gives satisfactory results for *Re* number higher than 0.2, which corresponds to flow rates higher than 100 μL/min.

(3) Synthesis of L-lactate using electroregenated NADH

Experimental Results. Mass balance experiments were performed under potentiostatic conditions using the filter-press microreactor. $FADH_2$ produced at the gold cathode (Figure 1b) reacts chemically with NAD^+ to lead to NADH; then L-lactate is synthesized from reaction with the continuously electro-regenerated NADH on pyruvate (3).

The solution used as catholyte contains at least five compounds and constitutes a complex mixture of FAD (or/and $FADH_2$), NAD^+ (or/and NADH), FDH, L-LDH, pyruvate (or/and L-lactate). The electrolyzed solution obtained at the outlet of the microreactor was immediately ($5 < \Delta t < 10$ min) analyzed by HPLC as described previously, and the results (Table 2) show that pyruvate was converted into L-lactate. Experiments without recycling (Run 1) did not yield high conversion (<25%) of pyruvate; the short residence time was insufficient to allow chemical reactions (−2) and (3) to take place, so the electrolyzed solution at the outlet of the reactor contained unreacted $FADH_2$ (which rapidly disappears by reaction with oxygen) as well as unreacted NADH. The quantities of these compounds were not determined because of the small volumes of solution involved (used for L-lactate HPLC analysis).

Quartering the flow, multiplying the LDH content by 2.5, and recycling the catholyte (ratio 0.25) increased the conversion of pyruvate to L-lactate (Run 2). Overall flow within the microreactor was decreased in comparison with Run 1. The consequence on the electrochemical reaction (1), performed under potentiostatic conditions, is the decrease in the resulting current, because flow acts directly on flavin (FAD) mass transfer. A low concentration of electroregenerated $FADH_2$ could lead to the drop in both NADH and pyruvate conversion. In fact conversion of pyruvate to L-lactate increases from 23 to 36%, indicating that

– the electrochemical reaction is not the limiting step and
– the increase in the residence time as well as in the LDH content increase the progression of both chemical reactions (−2) and (3).

Runs 3 and 4, performed without continuous recycling, confirm that it is the chemical reactions that are the rate-limiting steps; electrolyzed solution is collected at the outlet of the reactor, and after few minutes it is introduced within the reactor and electrolyzed again (three times). HPLC indicates quantitative conversion of pyruvate to L-lactate in these conditions.

The overall production rate of L-lactate can reach 0.13 mol/(m^2 day), a relatively low value because of the low concentrations of NAD^+ and FAD used. Even though these preliminary results are satisfactory, concentrations of substrate and enzymes have to be optimized, in order to increase their overall turnover number and the flux produced, as well as having an economically viable process (FDH: 100 €/100 U and L-LDH: 0.13 €/100 U). The experimental results obtained show that in these conditions, the maximum concentration of FDH must not exceed 0.005 U/cm^3, and for LDH the optimum value is 0.03 U/cm^3.

Simulation Results. Figure 10 reports three graphs giving the theoretical results obtained for the overall reaction scheme (Figure 1b) occurring in the microreactor. The same conditions as those used in the NADH regeneration section was applied for the synthesis of L-lactate. The pyruvate concentration was fixed at 3 mol/m^3.

Graph (a) gives the theoretical profiles of the normalised concentrations of the various compounds contained within the electrolyzed solution against microchannel length. Curves 1 and 2 represent FAD and $FADH_2$ concentrations, respectively. For one residence time, conversion of FAD to the reduced form reaches about 95%; the $FADH_2$ produced is not consumed by chemical reaction (−2) but accumulates within the microreactor. The outlet concentration of $FADH_2$ is about 14 times higher than the concentration of FAD as confirmed by graph (b).

Behavior similar to that of flavin is observed with the system NAD^+/NADH (Curves 3 and 4, graph a) as well as with the system puryvate/L-lactate (Curves 5 and 6, graph a).

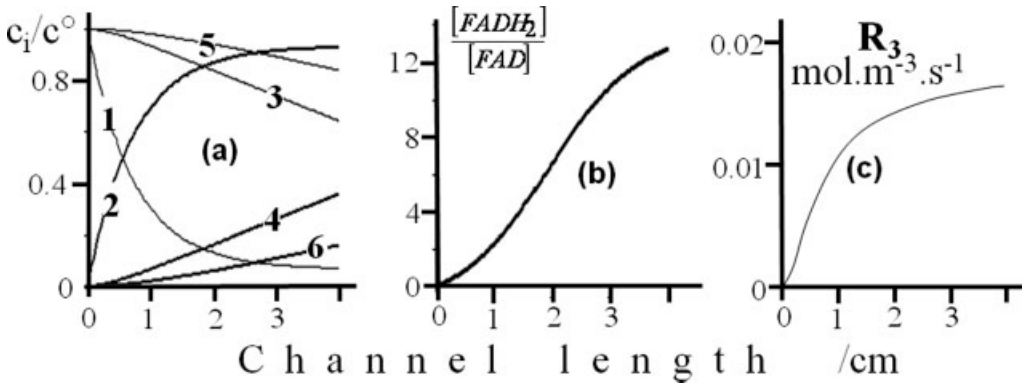

Figure 10. Simulated results of electrolyses performed using a filter press microreactor.

$[FAD]^\circ = [NAD^+]^\circ = 4$ mM; [pyruvate]$^\circ = 3$ mM $Q_{anolyte} = Q_{catholyte} = 0.0945$ cm^3/min; $R_{max-2} = 0.1$ mol/(m^3 s), $R_{max\ 3} = 0.02$ mol/(m^3 s). (a) Dimensionless concentration as a function of the microchannel length for all species, i.e., 1: FAD; 2: $FADH_2$; 3: NAD^+; 4: NADH; 5: Pyruvate; 6: L-Lactate. (b) Evolution of the simulated ratio $[FADH_2]/[FAD]$ within the microreactor. (c) Theoretical evolution of the chemical reaction NADH/pyruvate rate (R_3) vs. the microchannel length.

Conversions of NAD^+ and pyruvate reached ~40 and ~20%, respectively, for one residence time, indicating that the electrochemical step is faster than chemical reactions (−2) and (3) which are the rate-limiting steps of the overall process. As indicated in the Experimental section, low residence times do not allow chemical reactions (−2) and (3) to make much progress, so the electrolyzed solution at the outlet of the reactor contains, theoretically, unreacted $FADH_2$, NADH, and pyruvate. In these conditions, the flow rate as well as the temperature is the key parameters to optimize, in order to take account of the overall size of the filter-press electrochemical microreactor.

Graph (c) indicates the theoretical profile of the rate of R_3 vs. the microchannel length. A continuous augmentation of this rate was observed for microchannel lengths lower than 2 cm. Increasing the length allows R_3 to reach a steady state value [0.015 mol/(m^3 s^1)], three times lower than the value of R_{-2} for the NADH regeneration.

Optimally the steady-state value should be reached in the first part of the microchannel, which will maximize L-lactate production.

The simulated conversion of pyruvate to L-lactate is presented in Figure 6 (solid line, Curve 2). Experimental result obtained for Run 1 (Table 2) is also represented (●); incertitude on this measurement is mainly due to the HPLC analysis and corresponds to an error on the L-lactate concentration lower than 5%. Unfortunately, owing to the absence of experimental results in a large flow range, comparison with lower flows is not possible.

As observed for reaction (−2), conversion of pyruvate decreased as the flow increased; reduction in the residence time of the solution in the microreactor lowered both chemical rates (R_{-2} and R_3) which accounts for the behavior noted.

Conclusion

Previous work[17] allowed us to design and create, by electroerosion, a filter-press electrochemical microreactor, having a high specific area (250 cm^{-1}), enabling a practically quantitative conversion in the case of a single electrochemical reaction. In addition, this device was used to demonstrate that lowering the size of the electrolytic compartment authorized a nonthermodynamically favored reaction to take place. The electroenzymatic regeneration of NADH using a flavinic redox mediator is selected because the pyridinic cofactor NADH can be used for synthesis of several chiral compounds; reduction of pyruvate to L-lactate catalyzed by lactate dehydrogenase is chosen as model reaction.

Firstly, the tolerated range of flow-rates of this microreactor was determined; results ($0.001 < \text{flow} < 5$ cm^3/min) clearly demonstrate the necessity to improve the shape of the microreactor, particularly concerning the main input and output channels, in order to have a uniform velocity profile in all microchannels.

Secondly, mass balance measurements were used to optimize operating conditions, demonstrating that NADH is regenerated with conversions of 50%. This pyridinic cofactor is used to convert pyruvate into L-lactate, which was obtained with yields higher than 20%. Batch recycling of the treated solution (three times) led to complete transformation of the pyruvate, even if turnover numbers remain low (TTN ~ 1; TN ~ 80 h^{-1}).

Experimental results indicate that the 1-day production of L-lactate can reach 0.13 mol/m^2 of electrode area. It can be noted that the current microreactor can also be used for applications involving concentrated solutions, so production should increase significantly.

Theoretical modeling and simulation of the microreactor was performed using commercial software (FEMLAB); firstly ferri/ferrocyanide was used as model redox system to characterize the hydrodynamics as well as the electrochemical performances of the microreactor. Comparison of experimental and theoretical results validated various assumptions we had made.

Then, NADH regeneration and the overall chemical process described in Figure 1b was studied step by step. The previous model was modified to take into account both heterogeneous (1) and enzymatic (−2, 3) reactions. The theoretical results show that the Gibbs energy ΔG_{-2} is negative practically immediately at the inlet of the microchannel, demonstrating the high efficiency of the microreactor to create the conditions necessary to make a thermodynamically unfavorable reaction feasible.

The experimental operating conditions were not completely optimized, so the steady-state rates of enzymatic reactions R_{-2} and R_3 reached 0.045 and 0.015 mol/(m^3 s^1), respectively. Moreover, the concentration of the reduced forms $FADH_2$ and NADH increased against the length of the microchannel, and electrolyzed solution left the microreactor containing unreacted mediator as well as pyridinic cofactor.

Assuming the size of the microchannel to be constant, then flow, flavin and NAD^+ concentrations, as well as temperature are the parameters to be optimized to enable operation under maximum production conditions. Moreover, for the process to be economically valid, the enzyme quantities have to be optimized and reduced; one possibility could be the immobilization of FDH into a porous polymer support inside the microchannel; another possibility is to create a immobilized nanolayer using specific binding agents.

Finally, the shape and the size of both top and bottom channels has to be optimized to reduce velocity heterogeneities in the various microchannels.

Acknowledgments

We thank Alain Bergel from the "LGC UMR CNRS5503," for initiating this work, and Paul Kenis for his contributions and very helpful discussions.

Notation

α = cathodic electron transfer coefficient
A = absorbance
c = molar concentration (mol/m^3)
D = diffusion coefficient (m^2/s)
d_h = hydraulic diameter (m)
ε = molar absorptivity (L/mol cm)
E = potential (V)
ΔG, ΔG^0 = Gibbs energy and standard Gibbs energy (kJ/mol)
F = Faraday constant = 96 487 C/mol
FAD = flavin adenine dinucleotide
$FADH_2$ = reduced form of flavin adenine dinucleotide
FDH = formate dehydrogenase
η = overpotential (V)
HPLC = high-performance liquid chromatography
i_0 = exchange current density (A/m^2)
I and i = current (A) and current density (A/m^2)
k_{cat} = catalytic constant (s^{-1})
K_{av} = average mass transfer coefficient (m/s)
K_m = Michaelis-Menten constant (mol/m^3)
l and L = length of UV cell or microchannel (m)
LDH = lactate dehydrogenase
μ = dynamic viscosity (Pa s)
n = electron number
NAD^+ = nicotinamide adenine dinucleotide
N_j = molar flux density for species j [mol/(m^2 s)]
p = pressure (Pa)
Pe = Peclet number
Q = volumetric flow rate (m^3/s)
ρ = density (kg/m^3)
r = radius of the hemicylindrical microchannels
R = gas law constant = 8.31 J/(mol K)
Re = Reynolds number
R_j = reaction rate for species or reaction j [mol/(m^3 s)]
$R_{max\ j}$ = maximum rate of enzymatic reaction [mol/(m^3 s)]
S = electrode area (m^2)
τ = residence time
T = temperature (K)
TN = turnover number (s^{-1})
$$= \frac{\text{mol of product}}{\text{initial number of mol of cofactor} \times \text{operating time}}$$
$$\text{TTN} = \text{total turnover number} = \frac{\text{mol of product}}{\text{initial number of mol of cofactor}}$$
U = enzyme unit (quantity of enzyme able to transform 1 μmol of the substrate/min at 37°C)
V = velocity (m/s)
X = conversion (%)
x = channel length

Literature Cited

1. Dixon M, Webb EC. *Enzymes*, 3rd ed. New York: Academic Press, 1979.
2. Chenault HK, Whitesides GM. Regeneration of nicotinamide cofactors for use in organic synthesis. *Appl Biochem Biotechnol*. 1987;14:147–194.
3. Chenault HK, Simon ES, Whitesides GM. Cofactor regeneration for enzyme-catalysed synthesis. *Biotech Gen Eng Rev*. 1988;6:221–270.
4. Van der Donk WA, Zhao HM. Regeneration of cofactors for use in biocatalysis. *Curr Opin Biotechnol*. 2003;14:583–589.
5. Van der Donk WA, Zhao HM. Recent developments in pyridine nucleotide regeneration. *Curr Opin Biotechnol*. 2003;14:421–426.
6. Cantet J. Procédés de régénération du cofacteur pyridinique NADH par l'emploi simultanée d'une électrode et d'une hydrogénase, PhD Thesis, Toulouse, France, 1992.
7. Jaegfeldt H. Study of the products formed in the electrochemical reduction of nicotamide adenine dinucleotide. *Bioelectrochem Bioenerg*. 1981;8:355–370.
8. Ruppert R, Herrmann S, Steckhan E. Efficient indirect electrochemical in-situ regeneration of NADH: electrochemically driven enzymatic reduction of pyruvate catalyzed by d-LDH. *Tetrahedron Lett*. 1987;28:6583–6586.
9. Dicosimo R, Wong CH, Daniels L, Whitesides GM. Enzyme-catalysed organic synthesis: cofactors for use in organic electrochemical regeneration of NAD(P)H from NAD(P) using methyl viologen and flavoenzymes. *J Org Chem*. 1981;46:4622–4625.
10. Elving PJ, Bresnahan WT, Moiroux J, Samec Z. NAD/NADH as a model redox system: mechanism, mediation, modification by the environment. *Bioelectrochem Bioenerg*. 1982;9:365–378.
11. Samec Z, Bresnaham WT, Elving PJ. Theoretical analysis of electrochemical reactions involving two successive one-electron transfers with dimerization of intermediate-application to NAD^+/NADH redox couple. *J Electroanal Chem*. 1982;133:1–23.
12. Aizawa M, Coughlin RW, Charles M. Electrochemical regeneration of the reduced form NADH from the immobilised NAD^+. *Biotechnol Bieng*. 1976;18:209–215.
13. Gros P, Zaborosch C, Schlegel HG, Bergel A. Direct electrochemistry of *Rhodococcus opacus* hydrogenase for catalysis of NAD^+ reduction. *J Electroanal Chem*. 1996;405:189–195.
14. Cantet J, Bergel A, Comtat M. Coupling of the electroenzymatic reduction of NAD^+ with a synthesis reaction. *Enzyme Microbiol Technol*. 1996;18:72–79.
15. Bergel A, Comtat M. Thin-layer spectroelectrochemical study of the reversible reaction between nicotinamide adenine dinucleotide and flavin adenine dinucleotide. *J Electroanal Chem*. 1991;302:219–231.
16. Bergel A, Comtat M. Reduction of $NAD(P)^+$ by electrochemically driven $FADH_2$ and $FMNH_2$. *Bioelectrochem Bioenerg*. 1992;342:495–500.
17. Tzedakis T, Kane C, Launay A, Microréacteur. French Patent 04.12305, 2004, US Patent 2006/0108215A1, PCT 2006, WO 2006/053962.
18. Choban ER, Waszczuk P, Tzedakis T, Kenis PJA, Yoon SK, Kane C. Microfluidic Device and Synthetic Methods. US Patent 10/844,058, 2004.
19. Wienkamp R, Steckhan E. Indirect electrochemical regeneration of NADH by a bipyridinerhodium(I) complex as electron-transfer agent. *Angew Chem Int Ed Engl*. 1982;21:782–783.
20. Peguin S, Soucaille P. Modulation of metabolism of *Clostridium acetobutylicum* grown in chemostat culture in a three-electrode potentiostatic system with methyl viologen as electron carrier. *Biotechnol Bioeng*. 1996;51:342–348.
21. Simon H, Bader J, Günter H, Neumann S, Thanos J. Chiral compounds synthesized by biocatalytic reductions. *Angew Chem Int Ed Engl*. 1985;24:539–553.
22. Kashiwagi Y, Yanagisawa Y, Shibayama N, Nakahara K, Kurashima F, Anzai J, Osa T. Preparative, electroenzymatic reduction of NAD^+

to NADH on a thin poly(acrylic acid) layer-coated graphite felt electrode coimmobilizing ion-paired methyl viologen-cation-exchange polymer and diaphorase. *Chem Lett.* 1996;12:1093–1094.
23. Delecouls K, Saint-Aguet P, Zaborosch C, Bergel A. Mechanism of the catalysis by alcaligenes eutrophus H16 hydrogenase of direct electrochemical reduction of NAD^+. *J Electroanal Chem.* 1999;468:139–149.
24. Haswell SJ, Middleton RJ, O'Sullivan B, Skelton V, Watts P, Styring P. The application of micro reactors to synthetic chemistry. *Chem Commun.* 2001;5:391–398.
25. Löwe H, Ehrfeld W. State-of-art in microreaction technology: concepts manufacturing and applications. *Electrochimica Acta.* 1999;44:3679–3689.
26. Jähnish K, Hessel V, Löwer H, Baerns M, Chemistry in micostructured reactors. *Angew Chem Int Ed Engl.* 2004;43:406–446.
27. Mengeaud V. Design and characterisation of basic units for an electrochemical processing plant at the microscale, PhD Thesis No 2819, EPFL, Lausanne, Switzerland, 2003.
28. Xia YN, Whitesides GM. Soft lithography. *Angew Chem Int Ed.* 1998;37:551–575.
29. Fox RW, McDonald AT, Pritchard PJ. *Introduction to Fluid Mechanics*, 6th ed. Hoboken: Wiley, 2003.
30. Kim MJ, Whitesides GM. L-Lactate dehydrogenase: substrate specificity and use as a catalyst in the synthesis of homochiral 2-hydroxy acids. *J Am Chem Soc.* 1988;110:2959–2964.
31. Sun JJ, Xu JJ, Fang HQ, Chen HY. Electrocatalytical oxidation of NADH with dopamine covalently bound to self-assembled cysteamine monolayers on gold electrode. *Bioelectrochem Bioenerg.* 1997;44:45–50.
32. van der Wielen LAM, Zomerdijk M, Houwers J, Luyben KCAM. Diffusivities of organic electrolytes in water. *Chem Eng J.* 1997; 66:111–121.
33. Liquing R, Qu W, Dongqing L. Interfacial electrokinetic effect on liquid flow in microchannels. *Int J Heat Mass Transfer.* 2001;44: 3125–3134.
34. Wang YZG, Wang E. Electrochemical behavior of FAD at a gold electrode studied by electrochemical quartz crystal microbalance. *Anal Chim.* 1997;338:97–101.
35. Kane C. Conception et réalisation de microréacteurs électrochimiques- application à la régénération électroenzymatique de NADH et potentialités en synthèse, PhD Thesis, Toulouse, France, 2005.
36. Voet D, Voet J. Biochimie, traduction française de la. 2° édition de Gaudemer Y., Paris, Bruxelles: De Boeck Université, 1998.
37. Zewe V, Fromm HJ. Kinetic studies of rabbit muscle lactate dehydrogenase. *J Biol Chem.* 1961;237:1668–1675.
38. Tzedakis T, Savall A. Performance predictions in the scale-up of a liquid–liquid CSTR for indirect electro-oxidation of aromatic hydrocarbons. *Chem Eng Sci.* 1991;46:2269–2279.
39. Slusarczyk H, Felber S, Kula MR, Pohl M. Stabilization of NAD-dependent formate dehydrogenase from *Candida bodidinii* by site-directed mutagenesis of cysteine residues. *Eur J Biochem.* 2000;267: 1280–1289.

Annex: Analytical methods

Annex 1a: Enzyme assay

The activity of **FDH** from the yeast *Candida bodinii*, was determined by UV measurements; absorbance at 340 nm is correlated with the appearance of NADH during the oxidation of formate ion by NAD^+ according to:

$$HCO_2^- + NAD^+ \overset{FDH}{\rightleftharpoons} CO_2 + NADH \qquad (a1)$$

Operating conditions are as follows: 1 mol/m^3 of NAD^+, 50 mol/m^3 of HCO_2^-, 0.01 mg of FDH dissolved in 1 cm^{-3} of phosphate buffer at pH = 7.0. Specific activity of FDH is expressed in U_{FDH}/mg.

The activity of L-LDH from rabbit muscle was determined using the same method; the disappearance of NADH in the reaction with pyruvate (3) was followed at 340 nm. Operating conditions were the following: 2 mol/m^3 pyruvate; 50 mol/m^3 NADH and 5 U/cm^3 L-LDH. Specific activity of LDH is expressed in U_{LDH}/mg.

Units U_{FDH} (or U_{LDH}) being defined as the quantity of enzyme FDH (or L-LDH) enabling the appearance of 1 μmol of CO_2 (or L-lactate) per minute at 37°C.

Annex 1b: Spectrophotometric measurements

Flavin (FAD) and NADH samples were analyzed by UV/visible spectrophotometer in the wavelength range from 300 to 550 nm. The flavin (FAD) spectra contain two absorption bands with maxima at 450 and 375 nm. In the same range, the NADH spectrum presents one absorption bands at 340 nm. Calibrations for FAD and NADH were done at 340 and 450 nm using Beer-Lambert's law $A = \varepsilon \cdot l \cdot c$: where ε is molar absorptivity [L/(mol cm)]; l is the length of the UV cell (1 cm); and c is the concentration (mol/L). The molar absorptivity values at 340 nm are 4593 and 3663 L/(mol cm), respectively, for NADH and FAD. At 450 nm, NADH does not absorbs while absorbance is maximum for FAD and the corresponding molar absorptivity value is 7862 L/(mol cm), so the FAD concentration was estimated from this absorbance.

The determination of the NADH concentration in the electrolyzed solution needs another measurements of absorbance at 340 nm, which corresponds to the sum of absorbance of both FAD and NADH. The combination of these absorbance measurements allows the NADH concentration to be determined with incertitude lower than 4%.

Annex 1c: Chromatographic measurements

L-Lactate concentration was determined by HPLC and operated with an UV diode bar detector at 210 nm using sodium acetate as internal standard.

A nice resolution chromatogram is obtained, after experimental optimization, at 35°C, using a PL Hi-Plex H column from Polymer Laboratories. H_2SO_4 at 5 mol/m^3 used as eluent flows at 0.6 cm^3/min. Chromatogram indicates follow order for elution of various compounds and the corresponding retention time: [NAD^+], pyruvate, L-lactate and sodium acetate, respectively, at 6.5, 10.5, 14.0, and 16.2 min. In the chosen working conditions, the retention time of flavin and NADH was about 1 h.

Calibration of L-lactate, using sodium acetate as internal standard, led to the relationship (a2), and incertitude to this measurement led to an error on the L-lactate concentration lower than 5%.

$$\frac{A_{lactate}}{A_{acetate}} = 2.12\frac{[Lactate]}{[Acetate]} \qquad (a2)$$

Manuscript received Apr. 13, 2007, and revision received Jan. 19, 2008.